Supporting Information: The Many Faces of Heterogeneous Ice Nucleation: Interplay Between Surface Morphology and Hydrophobicity

Martin Fitzner,[1] Gabriele C. Sosso,[1] Stephen J. Cox,[1] and Angelos Michaelides[1]

London Centre for Nanotechnology, Department of Chemistry and Thomas Young Centre, University College London, 20 Gordon Street, London WC1H 0AJ, United Kingdom

CONTENTS

A. Distribution of the $\bar{q}_3(i)$ Order Parameter S2

B. Compressed Exponential Fit S3

C. Critical Nucleus Size on the (111) surface S4

D. Snapshots of Classified Regions S5

E. Distribution of Pre-Critical Nuclei S8

F. Notes on the Water Model S11

G. Higher Temperatures S14

Supplementary References S16

A. Distribution of the $\bar{q}_3(i)$ Order Parameter

Nucleation was monitored by following the change in the potential energy. As a separate check, for selected trajectories we also monitored N_{cls}, the number of molecules in the largest solid-like cluster. The state of molecules was characterized by a modified version of the local $\bar{q}_3(i)$ parameter[1]. Figure S1 shows the distribution of $\bar{q}_3(i)$ for different phases. We applied a cutoff of 3.2 Å for both the $\bar{q}_3(i)$ neighbor-list and the cluster algorithm.

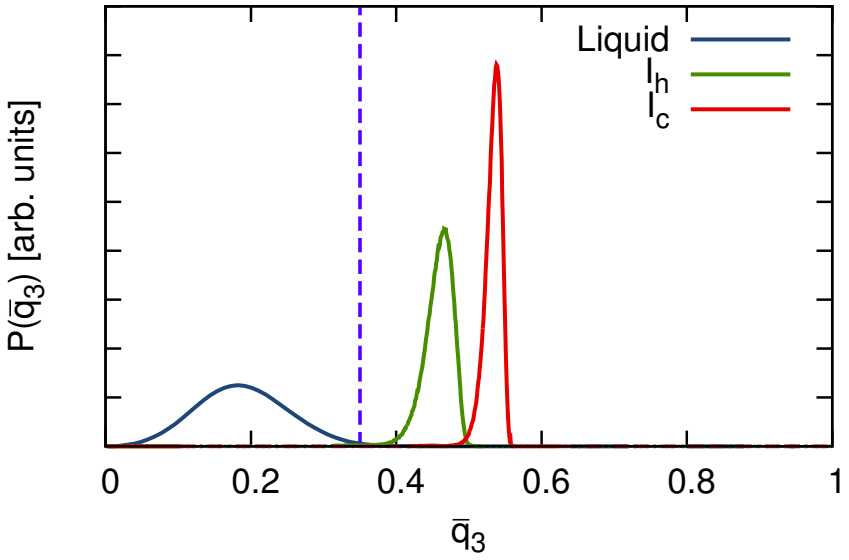

FIG. S1. Distribution for the $\bar{q}_3(i)$ parameter for liquid water, hexagonal ice I_{h} and cubic ice I_{c}. The data was obtained by a short time simulation of the liquid and pristine crystals respectively (205 K, 4096 molecules, NPT, 10 ns). The dashed line indicates the threshold above which particles have been considered as solid.

B. Compressed Exponential Fit

The simulation protocol involves an instantaneous quench from the equilibration temperature to the one at which we study nucleation. Because the system has to relax into quasi-equilibrium first, the nucleation rate increases with time, resulting in a deviation from perfect exponential characteristics. The effect of this non-exponential behavior can be appreciated in Figure S2, where we show the $t_{\rm n}$ datasets and the resulting $P_{\rm liq}(t)$ for two dissimilar nucleation scenarios observed on the (110) surface as a function of the strength of the water-surface interaction. In the case of a) the nucleation typically proceeds on a timescale ranging from 1 to 100 ns, resulting in well behaved exponential decay ($\gamma \sim 1$ in equation 4 for the survival probability). On the other hand, the fitting of the data shown in Figure S2b gave $\gamma \gg 1$, which in turn implies a nucleation rate that increases with time, as the timescale for $t_{\rm n}$ (0.1-1 ns) is indeed comparable with the relaxation time of the system. This occurrence takes place mainly for those ($E_{\rm ads}$,$a_{\rm fcc}$) values for which we observe the basically instantaneous (10-1000 ps) formation of almost perfect ice-like overlayers on top of the surface.

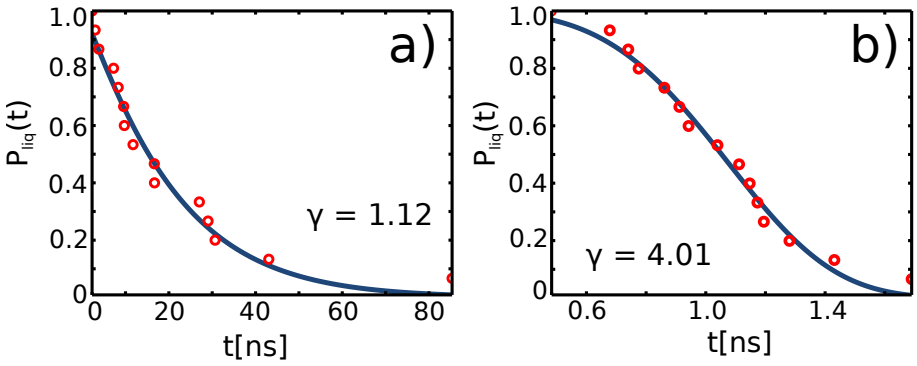

FIG. S2. Compressed exponential fitting results for two dissimilar nucleation events. $P_{\rm liq}(t)$ (red circles) and fit after equation 4 (blue lines) for the (110) surface and $a_{\rm fcc} = 3.9$ Å. a) $E_{\rm ads} = 11.63$ kcal/mol and b) $E_{\rm ads} = 5.3$ kcal/mol.

C. Critical Nucleus Size on the (111) surface

To obtain an estimate of the critical nucleus size we performed a committor analysis[2] on the (111) surface. The results are depicted in Figure S3 and suggest a critical nucleus size of circa 50 mW molecules, which is much smaller than our system size (4000 mW).

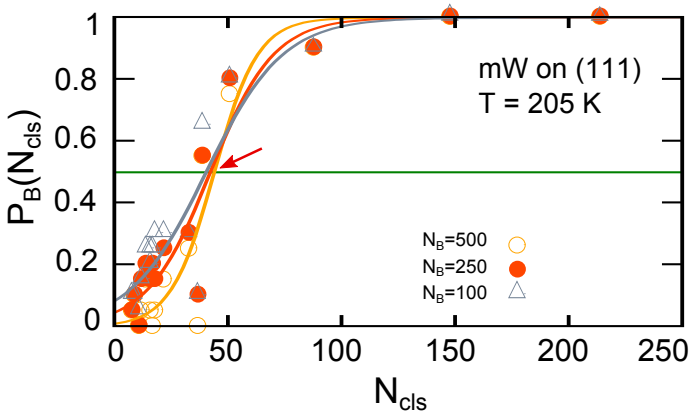

FIG. S3. Committor probability (P_B) with respect to the number $N_{\rm cls}$ of mW molecules in the biggest ice-like cluster for the (111) surface ($E_{\rm ads} = 1.04$ kcal/mol, $a_{\rm fcc} = 3.90$ Å). Three different thresholds $N_{\rm B}$ for the order parameter have been considered and reported. The analysis has been obtained by shooting 30 statistically independent MD runs (2 ns long) from 40 different starting configurations taken along a nucleation trajectory. The arrow marks the critical nucleus size ≈ 50.

D. Snapshots of Classified Regions

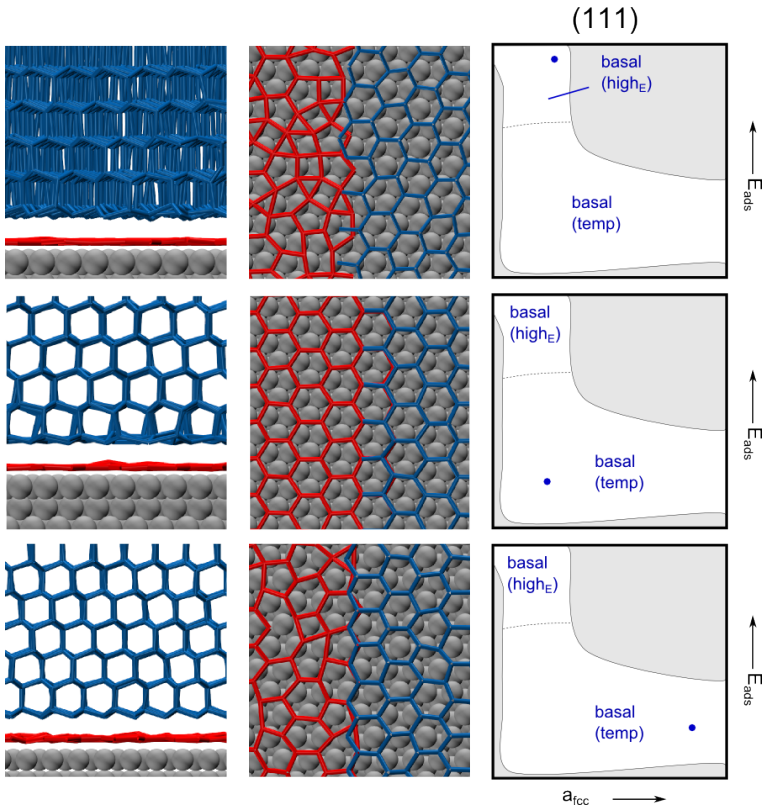

FIG. S4. Classified regions for the 111 surface. Snapshots are taken from regions indicated by the blue dot.

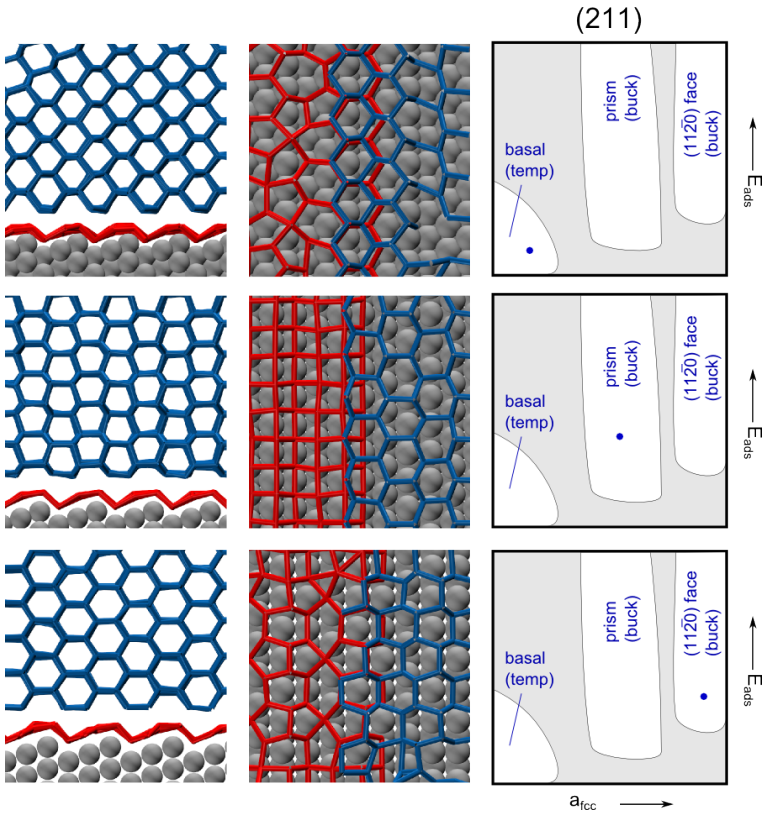

FIG. S5. Classified regions for the 211 surface. Snapshots are taken from regions indicated by the blue dot.

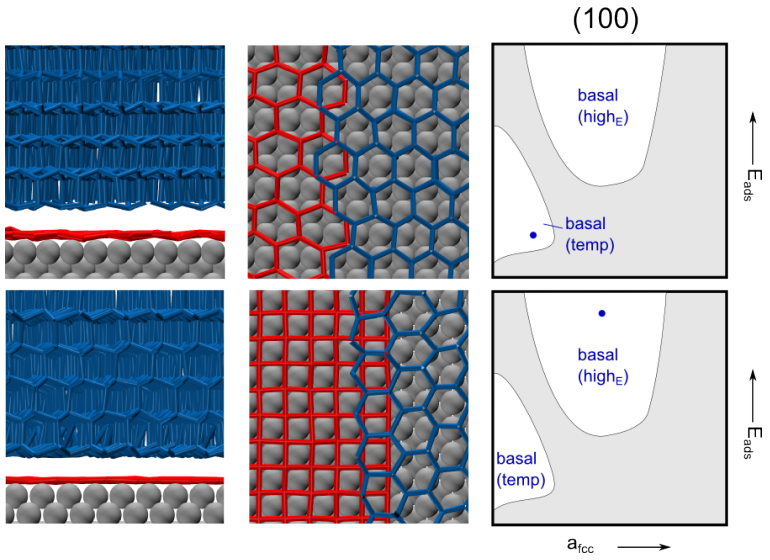

FIG. S6. Classified regions for the 100 surface. Snapshots are taken from regions indicated by the blue dot.

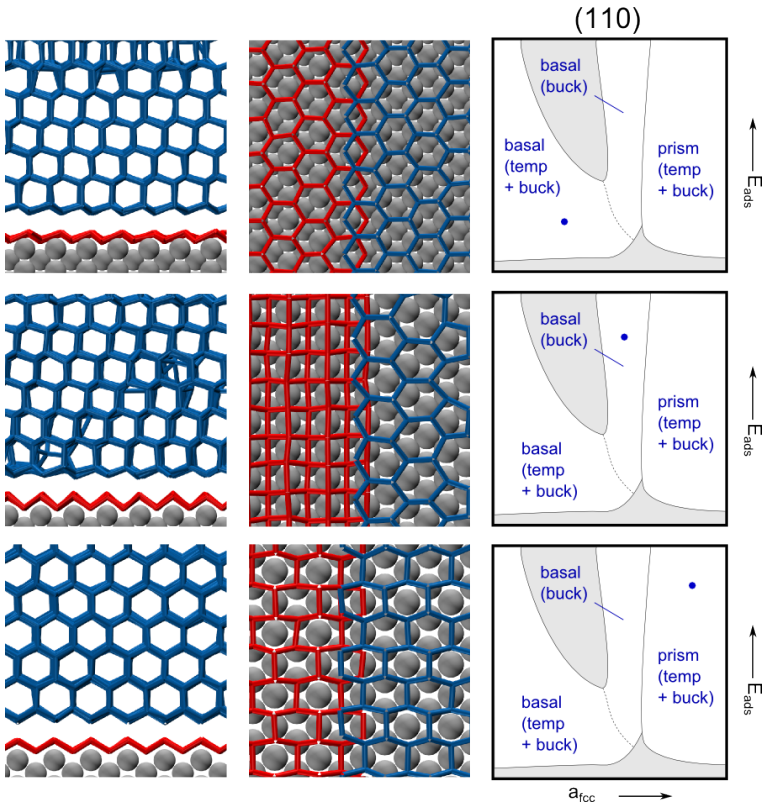

FIG. S7. Classified regions for the 110 surface. We note that the side view of the last region does not show the typical side perspective of the prism face. However, it results from a 90° rotation around the z axis of the typical view, as seen e.g. in the prism region of the (211) surface. Snapshots are taken from regions indicated by the blue dot.

E. Distribution of Pre-Critical Nuclei

The distribution of pre-critical nuclei in Figure S8 is helpful for discussing what is the only common feature found for all of the four surfaces: inhibition of the nucleation rate for the smallest value of E_{ads}. For this interaction strength the molecules essentially face a hard wall which in turn could even hinder nucleation compared to the homogeneous case[3–6]. To understand this we must first mention, what happens for the homogeneous bulk case (which we term Homo) and the case of a free standing water slab (called $\mathrm{Homo_{VAC}}$) with two water-vacuum interfaces. The nucleation rate of $\mathrm{Homo_{VAC}}$ will be lower than in the bulk case (Homo), which can be roughly rationalized in terms of a smaller volume available for the nuclei to appear than in the bulk case. This effect is visible in Figure S8, where the distribution for Homo corresponds to a constant line, while the probability for $\mathrm{Homo_{VAC}}$ is decreased towards the interface. In fact, the nucleation rate constant for $\mathrm{Homo_{VAC}}$ computed by excluding the volume of the system affected by the presence of the water-vacuum surface (which can be estimated by looking at the density profile along the z-coordinate, see SI Figure S9a) is basically the same as obtained for Homo. In the case of our models, the presence of the LJ surface could introduce significant density perturbations in the water film for all values of E_{ads} (see SI Figure S9b). As a result, when no efficient template can be provided by the surface, pre-critical nuclei tend to strictly avoid the neighborhood of the LJ surface as well, as reported in Figure S8 (Inh). This effect could be even stronger than the inhibition coming from the water-vacuum interface, and as a result the effective volume available for the nuclei to appear is even less than in the $\mathrm{Homo_{VAC}}$ case, thus causing a net inhibiting effect due to the presence of the surface. It is worth noting that while the promotion of the nucleation rate observed for many (a_{fcc},E_{ads}) points can be rather strong, the inhibition effect is usually much weaker, as it basically accounts for the removal of the portion of the system affected by the presence of the LJ surface. This kind of inhibition is therefore unlikely to be visible in simulations or experiments where the ratio of water volume to contact area is much higher than in our case.

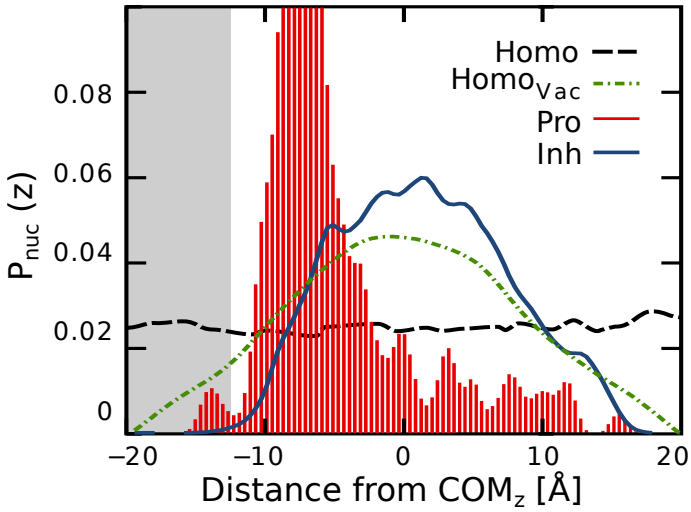

FIG. S8. Probability density distribution $P_{\mathrm{nuc}}(z)$ of the z-coordinate of center of mass (COM) of pre-critical ice-like clusters. The x-axis refers to the distance from the COM of the mW water slab. The gray shaded region highlights the extent of the 1st and 2nd water overlayer on top of the LJ surface. The legend refers to a bulk model of 4000 mW molecules (Homo), the same as a free-standing slab ($\mathrm{Homo_{VAC}}$) and scenarios (Inh and Pro) in which we observe inhibition/promotion of J on the (100) surface ($a_{\mathrm{fcc}} = 3.90$ Å for both, $E_{\mathrm{ads}} = 3.21$ and 5.30 kcal/mol respectively). All data was collected at 205 K.

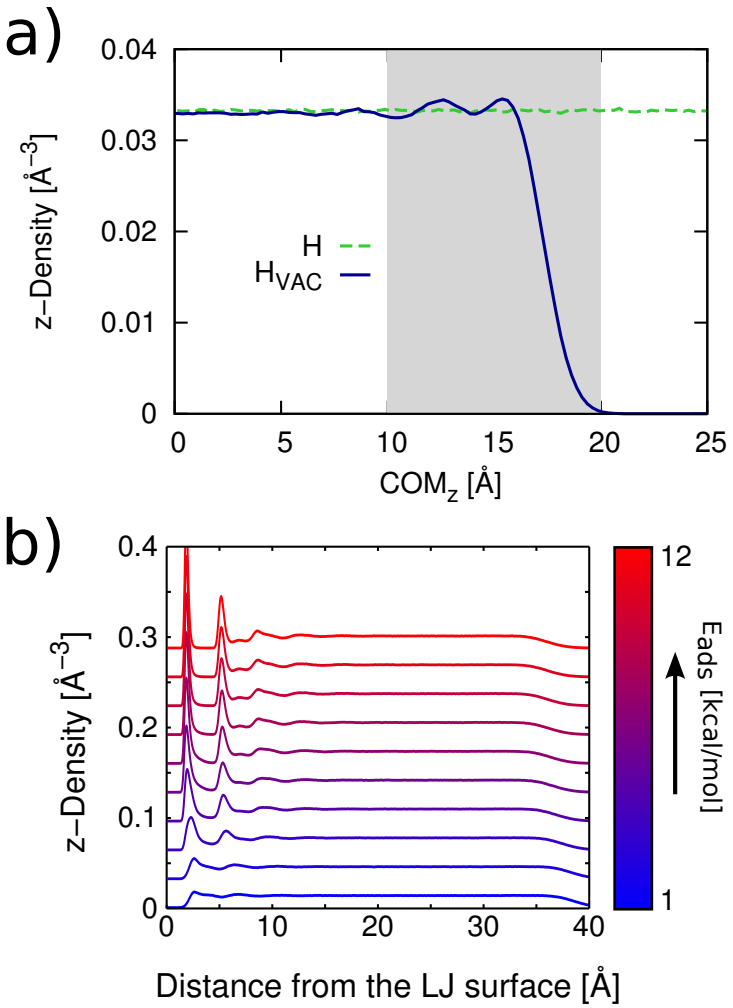

FIG. S9. a) z-Density profile of a homogeneous mW model (4000 molecules) H and the same model as a free standing slab (H_{VAC}), featuring two water-vacuum interfaces. The x-axis refers to the distance from the center of mass of the mW slab along the z coordinate (only one side of the slab is shown). The shaded region highlights the fraction of the system affected by the presence of the water-vacuum interface because of density oscillations. b) z-Density profile of mW water on top of the (100) surface ($a_{\mathrm{fcc}} = 3.9$ Å, obtained at 290 K) as a function of E_{ads}.

F. Notes on the Water Model

Firstly, we checked that the water densities observed (e.g. depicted in Figure 6) are not an artifact of the coarse grained water model by comparing them to the results of TIP4P/2005. The test was done for one (a_{fcc},E_{ads}) point on each surface. The water-surface interaction was kept identical to the mW case, i.e. the surface atoms interact with the TIP4P/2005 oxygens through the same LJ potential. The resulting densities (see Figure S10) are very similar. While the the latter shows slightly stronger peaks and layering, the peak positions agree with the mW values. We conclude that the structuring exhibited by the mW model is nearly equivalent to the one of TIP4P/2005. Our results concerning the buckling and the structuring perpendicular to the surface should therefore be applicable to all-atom models of water. It appears that potential differences for overlayer patterns obtained from simulations are artifacts of the very different time scales on which both models evolve rather than actual structural differences.

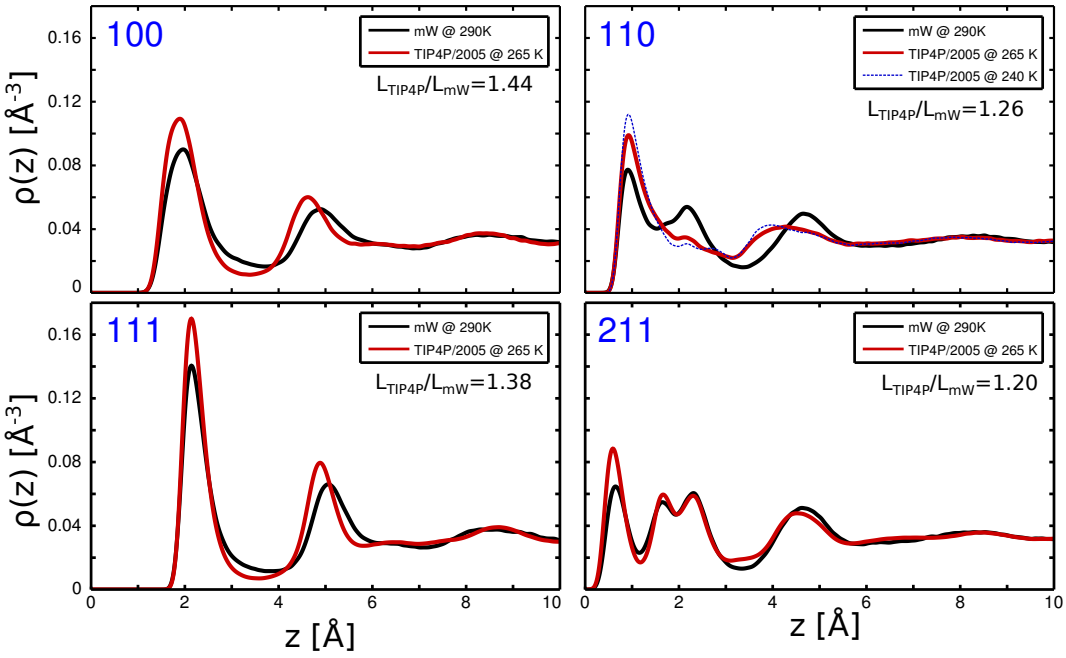

FIG. S10. Comparison of the density perpendicular to the surface for the mW and TIP4P/2005 models of water. Results are based on at least 75 ns long equilibration trajectories approximately 15 K above the melting point of the corresponding model. All graphs were computed for $a_{\mathrm{fcc}} \approx 3.9$ Å and $E_{\mathrm{ads}} \approx 3.2$ kcal/mol. The temperature was chosen to be approximately 15 K above the melting point of the respective water model.

Secondly, we performed nucleation simulations with TIP4P/2005 water on the (111) surface for a_{fcc}=3.90 Å and different values of E_{ads}. Contrary to the mW case, using the all-atom model we did not observe the formation of a complete hexagonal overlayer within 100 ns. This might not seem a surprise, specifically because of the lack of a hydrogen bond network. This deficiency results in a much faster dynamics (we have estimated a mismatch in the self-diffusion coefficient of about three orders of magnitude at the supercooling considered here) of the water molecules with respect to both experiments and basically any full atomistic water model[7,8]. Besides, the mW model potential energy surface is much smoother than one in which hydrogen bonds would be taken into account. However, the number and the size of hexagonal patches within the first overlayer is consistent with what we have observed in the case of the mW model. In Figure S11 we report the probability density function of the size of the biggest hexagonal patch of TIP4P/2005 water molecules on top of the (111) surface. The tails of the distributions, corresponding to sizable hexagonal patches can only be observed for E_{ads} = 3.2 kcal/mol, which is exactly the value for which we observe the fastest formation of the hexagonal overlayer in the case of mW. To gauge interaction energies for different water models the heat of vaporization is often used. The latter for both models is nearly the same[7,9] which means we can compare the adsorption energies directly. The trend holds for different supercooling as well, and confirms that while - especially heterogeneous - nucleation processes modeled by mW water are for certain nonphysically fast, the model could still capture part of the underlying physics of the problem.

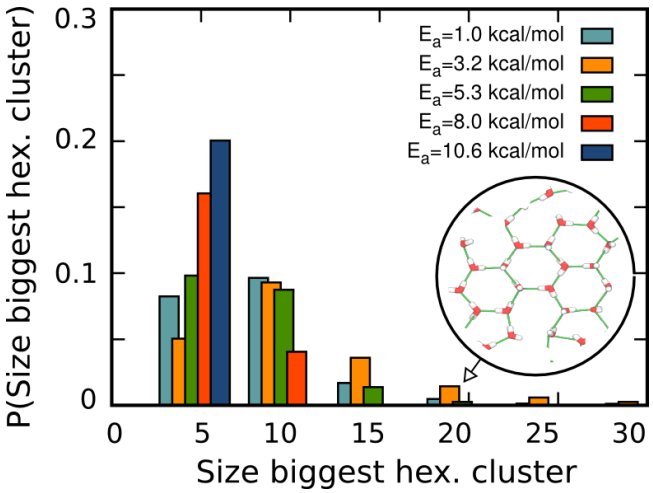

FIG. S11. Probability density distribution of the size of the biggest hexagonal patch of TIP4P/2005 water molecules within the first overlayer for different values of E_{ads} and a_{fcc}=3.90 Å on the (111) surface. Results were taken from 20 ns trajectories sampled with a 2 fs timestep. The inset depicts a fairly large cluster of about 20 molecules.

G. Higher Temperatures

Our simulations have been performed in the deeply supercooled regime. It is beyond reach to do such an extensive set of simulations as performed here at significantly higher temperature. Nonetheless it is interesting to understand how the phenomena observed might depend on temperature. To estimate the effect of the strong supercooling on the results and especially the proposed mechanisms we performed calculations at higher temperatures for three adsorption energies on the (110) surface (depicted in Figure S12). Since the computational cost significantly increases, the nucleation rates become less accessible with the brute force approach and we therefore limit this trial to only a few (a_{fcc},E_{ads}) points. As previously mentioned, the values at the top and bottom range of the nucleation rate should be seen as a lower/upper bound to the actual nucleation rate. Conclusively, a missing temperature dependence of these points indicates a nucleation rate out of the limit that can be resolved with simulations of 500 ns length, rather than one that is constant with temperature. We find that the trends seen at 205 K are stable against the temperature increase and only in regions where no specific mechanism has been attributed the rates heavily decline. In fact the increased temperature can help to identify the values of a_{fcc} inducing a certain mechanism in a more precise way because the gaps between the enhanced regions increase. Furthermore, the structures of the adsorption layers did not show any noticeable change so that we can assume that our conclusions are valid also for higher temperatures.

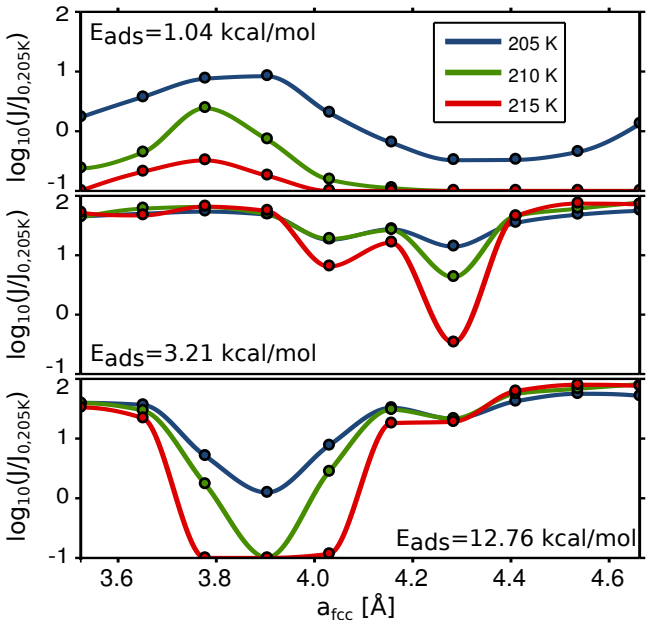

FIG. S12. Temperature dependence of nucleation rates (circles) and spline interpolation (colored lines) for 3 adsorption energies on the (110) surface. All values were normalized by the homogeneous nucleation rate J_0 at 205 K.

SUPPLEMENTARY REFERENCES

[1]W. Lechner and C. Dellago, J. Chem. Phys. **129**, 114707 (2008).

[2]P. G. Bolhuis, D. Chandler, C. Dellago, and P. L. Geissler, Annu. Rev. Phys. Chem. **53**, 291 (2002).

[3]A. Reinhardt and J. P. K. Doye, J. Chem. Phys. **141**, 084501 (2014).

[4]A. Haji-Akbari, R. S. DeFever, S. Sarupria, and P. G. Debenedetti, Phys. Chem. Chem. Phys. **16**, 25916 (2014).

[5]H. Zhang, S. Peng, L. Mao, X. Zhou, J. Liang, C. Wan, J. Zheng, and X. Ju, Phys. Rev. E **89**, 062410 (2014).

[6]H. Zhang, S. Peng, X. Long, X. Zhou, J. Liang, C. Wan, J. Zheng, and X. Ju, Phys. Rev. E **89**, 032412 (2014).

[7]V. Molinero and E. B. Moore, J. Phys. Chem. B **113**, 4008 (2009).

[8]M. Orsi, Mol. Phys. **112**, 1566 (2014).

[9]J. L. F. Abascal and C. Vega, J. Chem. Phys. **123**, 234505 (2005).